Dalton Transactions

Accepted Manuscript

ROYAL SOCIETY OF CHEMISTRY

www.rsc.org/dalton

Table of contents entry

Nine isostructural lanthanide metal–organic frameworks based on 1, 1'–ethynebenzene–3, 3', 5, 5' –tetracarboxylate ligand capable of emitting from the visible to near–infrared wavelengths have been synthesized and characterized in detail.

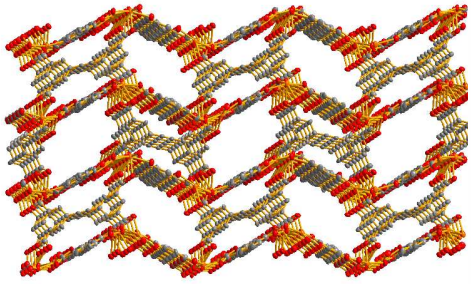

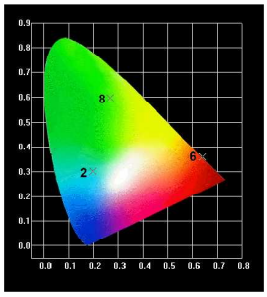

Ln = La (**1**), Ce (**2**), Pr (**3**), Nd (**4**), Sm (**5**), Eu (**6**), Gd (**7**), Tb (**8**) and Dy (**9**)

Luminescent lanthanide–MOFs with millisecond order lifetime based on conjugated 1, 1'–ethynebenzene–3, 3', 5, 5'–tetracarboxylate ligand: syntheses, structures and photoluminescent properties

Lu Zhai,[a,b] Wen–Wei Zhang,*[b] Xiao–Ming Ren*[a] and Jin–Ling Zuo[b]

[a] *State Key Laboratory of Materials–Oriented Chemical Engineering and College of Science, Nanjing Tech University, Nanjing 210009, P. R. China. E–mail: xmren@njtech.edu.cn*

[b] *State Key Laboratory of Coordination Chemistry, School of Chemistry and Chemical Engineering, Nanjing University, Nanjing 210093 P. R. China. E–mail: wwzhang@nju.edu.cn*

Abstract

A family of novel lanthanide metal–organic frameworks (MOFs) with formula $[Ln_2(EBTC)_{1.5}(CH_3OH)_4]\cdot 6H_2O$ [$EBTC^{4-}$ = 1, 1′–ethynebenzene–3, 3′, 5, 5′–tetracarboxylate，Ln = La (**1**), Ce (**2**), Pr (**3**), Nd (**4**), Sm (**5**), Eu (**6**), Gd (**7**), Tb (**8**) and Dy (**9**)], have been synthesized via solvothermal reaction. All compounds are isostructural, crystallized in monoclinic space group $P2_1/n$, and show three–dimensional (4, 6)–connected network with Schläfli symbol of $\{3^{10}\}$. Photoluminescent measurements indicated that **1** and **7** emit the luminescence originating from the intraligand π←π* transition, **2** shows the broad band emission due to allowed 4f–5d transitions, and **4**–**9** show the emission of typical lanthanide f–f transition via the ligand "antenna effect" in the solid state at ambient temperature. Interestingly, compounds **6** and **8** show microsecond time scale fluorescence lifetimes with 0.84 ms for **6** and 0.39 ms for **8**, respectively, such unique spectroscopy feature

may have an application in the research of biomacromolecule.

Keywords: Lanthanide coordination polymer, isostructural, antenna effect, microsecond time scale luminescence–lifetime

Introduction

Recently, metal–organic frameworks (MOFs) or coordination polymers (CPs) have been extensively studied in catalysis,[1] gas or molecule separation,[2] gas absorption and storage,[3] luminescence,[4] magnetism,[5] proton conductor,[6] ferroelectrics[7] and other application fields. By comparison of MOFs based on d–block transition metal ions, the design and control over multidimensional lanthanide MOFs (Ln–MOFs) have attracted more great interest owing to their well–known spectroscopic properties and specific coordination natures typically of lanthanide ions. The emission bands, originated from the electronic transitions within the well-shielded $4f^n$ configuration of the lanthanide ions, cover the visible and near to mid–infrared parts of the optical spectrum and show quite narrow half–wave width and corresponding compounds possess high color purity. However, in a centrosymmetric environment, the electronic transitions between like atomic orbitals such as s–s, p–p, d–d, or f–f, transitions are forbidden, and this leads to the existence of weak light absorption for the f–f transition of lanthanide ions. To enhance the f–f emission of lanthanide ion in a complex, a strategy, so-called 'antenna effect',[8] was developed. In such a case, it makes the energy level be matchable between the f–orbital of lanthanide ion and π*–orbital of ligand via rationally designing the molecular structure of a ligand, as a result, the excitation energy is efficiently transferred from the ligands to the lanthanide ions through intramolecular energy transfer.

The aromatic multicarboxylate is a candidate with good 'antenna effect' for sensitizing and enhancing the f–f luminescence of Ln^{3+} ion, up to date, lots of efforts have being dedicated toward the studies of luminescent MOFs of Ln^{3+} ions with aromatic multicarboxylate ligands.[9]

In previous study, we found that the π-conjugated multicarboxylate ligand, 1, 1'–ethynebenzene-3, 3', 5, 5'–tetracarboxylate (H_4EBTC) is an efficient 'antenna effect' ligand for enhancing Eu^{3+} emission of f–f transition.[10] In this contribution, we systematically investigated the crystal structures and luminescence properties for nine new $EBTC^{4-}$–based Ln–MOFs.

Experimental Section

Chemicals and reagents

N, N–dimethylformamide (DMF) and dimethylsulfoxide (DMSO) were dried and distilled according to standard procedures. $Ln(NO_3)_3 \cdot xH_2O$ (where Ln^{3+} = Pr^{3+}, Sm^{3+}, Eu^{3+}, Gd^{3+}, Tb^{3+} and Dy^{3+}) were prepared by the reaction of nitric acid with the corresponding lanthanide oxide. Other lanthanide nitrates, such as $La(NO_3)_3 \cdot 6H_2O$, $Ce(NO_3)_3 \cdot 6H_2O$ and $Nd(NO_3)_3 \cdot 6H_2O$, were purchased from chemical company and used directly. All commercially available chemicals were of analytical grade and used as received without further purification. H_4EBTC was synthesized according to the method published before.[11]

Physical measurements

Elemental analyses (C, H) were performed on a Perkin–Elmer 240 elemental analyzer. Thermal gravimetric analyses (TGA) were performed using a DTA–TGA 2960 thermogravimetric analyzer in nitrogen atmosphere with a heating rate of 20 °C/min. Powder X–ray diffraction (PXRD) data were recorded on a Shimadzu XRD–6000 diffractometer with Cu Kα (λ = 1.54056 Å) radiation at room temperature with a scan speed of 5 °/min and a step size of 0.02° in 2θ. The IR spectra were obtained on a NICOLET iS10 spectrometer with KBr pellets in the 4000–400 cm^{-1} region. The absorption spectra were got from Shimadzu UV–3600 spectrometer for the solid samples. Luminescence spectra were recorded for the solid samples on an F–4600 FL spectrophotometer equipped with a 150 W Xenon lamp as an excitation source at room temperature. The photomultiplier tube (PMT) voltage was 400 V in all the measurements. The scan speed was 1200 nm/min. The photoluminescence lifetime was measured with an Edinburgh Instruments FLS920P fluorescence spectrometer.

Preparation and characterization of Ln–MOFs

$[La_2(EBTC)_{1.5}(CH_3OH)_4] \cdot 6H_2O$ (1). A solution of $La(NO_3)_3 \cdot 6H_2O$ (13 mg, 0.03 mmol), H_4EBTC (5 mg, 0.014 mmol), DMSO (0.4 mL), CH_3OH (0.20 mL), HNO_3 (0.06 mL, 1M in DMF) and H_2O (0.10 mL) were mixed and sealed in a 10 mL

Teflon-lined autoclave and heated to 110 °C for 17 h. Colorless block-shaped crystals were achieved after slowly cooled to room temperature (yield: 75% based on La). Anal. Calcd for $C_{31}H_{29}La_2O_{18}$: C, 38.49; H, 3.00. Found: C, 38.13; H, 2.98. Selected IR data (KBr pellet, cm^{-1}): 3440 (m), 3065 (w), 3001 (w), 2918 (w), 1617 (s), 1572 (s), 1430 (s), 1378 (s), 1014 (s), 784 (m), 713 (m).

The analogous procedure above–mentioned was used for preparation of **2–9** (ref. ESI), just replaced $La(NO_3)_3$ by other $Ln(NO_3)_3$. The microanalysis, yield and main IR bands are summarized in Table 1.

Table 1 Elemental analysis, yield and main IR bands for **1**–**9**

Compound	Formula	C% (Found)*	H% (Found)	Yield%**	Main IR Bands
1	$C_{31}H_{29}La_2O_{18}$	38.49(38.13)	3.00 (2.98)	75%	3440m, 3065w, 3001w, 2918w, 1617s, 1572s, 1430s, 1378s, 1014s, 784m, 713m
2	$C_{31}H_{29}Ce_2O_{18}$	38.39(38.16)	2.99 (2.97)	72%	3438m, 3067w, 3004w, 2913w, 1626s, 1550s, 1436s, 1378s, 1018s, 786m, 717m
3	$C_{31}H_{29}Pr_2O_{18}$	38.33(38.23)	3.01 (3.03)	68%	3369m, 3072w, 3005w, 2915w, 1628s, 1559s, 1436s, 1375s, 1004s, 786m, 717m
4	$C_{31}H_{29}Nd_2O_{18}$	38.07(38.13)	2.99 (2.94)	62%	3394m, 3073w, 3001w, 2918 w, 1628s, 1559s, 1436s, 1375 s, 1011s, 786m, 717m
5	$C_{31}H_{29}Sm_2O_{18}$	37.60(37.34)	3.00 (2.84)	60%	3438m, 3067w, 3004w, 2914w, 1626s, 1550s, 1436s, 1378s, 1018s, 78 m, 71 m
6	$C_{31}H_{29}Eu_2O_{18}$	37.48(37.18)	2.92 (2.90)	65%	3470m, 3067w, 3003w, 2915w, 1626s, 1550s, 1436s, 1378s, 1018s, 786m, 717m
7	$C_{31}H_{29}Gd_2O_{18}$	37.08(36.75)	2.89 (2.86)	60%	3421m, 3069w, 3004w, 2915w, 1626s, 1550s, 1440s, 1380s, 1014s, 786m, 717m
8	$C_{31}H_{29}Tb_2O_{18}$	36.96(36.63)	2.88 (2.65)	66%	3457m, 3070w, 3004w, 2912w, 1628s, 1558s, 1436s, 1378s, 1018s, 786m, 717m
9	$C_{31}H_{29}Dy_2O_{18}$	36.70(36.87)	2.88 (2.91)	61%	3438m, 3067w, 3003w, 2915w, 1628s, 1560s, 1448s, 1378s, 1016s, 786m, 718m

* Anal. Calcd for the formula and the experimental value in the parentheses; ** Yield was calculated based on the rare earth metal.

Crystallographic Analyses

Single crystal X–ray diffraction data were collected on a Bruker Smart Apex II CCD diffractometer at 291 K using graphite monochromated Mo/Kα radiation (λ = 0.71073 Å). Data reductions and absorption corrections were performed with the SAINT and SADABS software packages,[12] respectively. Structures were solved by a direct method using the SHELXL–97 software package.[13] The non–hydrogen atoms were anisotropically refined using the full–matrix least–squares method on F^2. All hydrogen atoms were placed at the calculated positions and refined riding on the parent atoms. It should be mentioned that (1) the crystallographic data of **1, 2, 3** and **7** are not good due to impossible getting the high quality of single crystals, and were shown in ESI; (2) the single crystal of **6** and **8** are too small to give the usable crystallographic data. The good crystallographic data were obtained for **4, 5** and **9**, and the corresponding data of collection and refinement details are presented in Table 2 for them. The CCDC reference numbers are 1037093, 1037094 and 1037095 for **4**, **5** and **9**, respectively.

Table 2 Crystallographic data and structural refinements for **4**, **5** and **9**

Compound	**4**	**5**	**9**
Formula	$C_{31}H_{29}Nd_2O_{18}$	$C_{31}H_{29}Sm_2O_{18}$	$C_{31}H_{29}Dy_2O_{18}$
Formula weight	978.02	990.240	1014.54
CCDC no.	1037093	1037094	1037095
Temperature (K)	291(2)	291(2)	291(2)
Wavelength (Å)	0.71073	0.71073	0.71073
Crystal size /mm	0.28×0.24×0.22	0.26×0.24×0.22	0.20×0.20×0.15
Crystal system	Monoclinic	Monoclinic	Monoclinic
Space group	*P2(1)/n*	*P2(1)/n*	*P2(1)/n*
a / *Å*	14.5952(12)	14.4388(18)	14.4821(18)
b / *Å*	16.7329(11)	16.4128(19)	16.7137(19)
c / *Å*	19.5713(14)	19.3310(12)	19.2130(12)
β / *Å*	107.344(3)	107.606(3)	108.039(3)
V / *Å*^{3}	4562.4(6)	4366.5(8)	4421.9(8)
Z	4	4	4
F(000)	1916	1932	1964
$\theta_{min,max}$/°	1.63–26.00	1.56–26.00	1.55–26.00
GOF	1.090	1.051	1.006
R_1, wR_2 [$I > 2\sigma(I)$][a]	0.0593, 0.1371	0.0589, 0.1407	0.0419, 0.0897

Results and Discussion

Crystal Structures. As shown in Fig. 1, the powder X–ray diffraction measurements revealed that **1–9** are isostructural with each other. The PXRD patterns of the bulk materials of **1–9** are in good agreement with the simulated ones of **4, 5** and **9** (Fig. S1, ESI†), confirming that the as-synthesized products of **1–9** show high phase purity. Besides this, the IR spectra of **1–9** are almost identical (ref. Fig. S2, ESI†), and the microanalysis disclosed that the nine compounds possess the analogous chemical components with a formula of $[Ln_2(EBTC)_{1.5}(CH_3OH)_4]\cdot 6H_2O$ (where Ln = La, Ce, Pr, Nd, Sm, Eu, Gd, Tb and Dy). As a result, herein, only the structure of $[Sm_2(EBTC)_{1.5}(CH_3OH)_4]\cdot 6H_2O$ (**5**) is representatively described in detail. The structure of **4** and **9** is shown in Fig. S3.

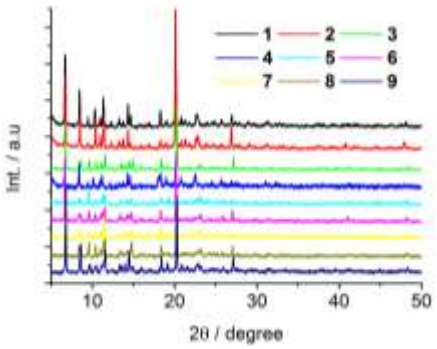

Fig. 1 PXRD patterns of **1–9** at ambient temperature.

Crystal of **5** belongs to monoclinic space group *P2(1)/n*. As shown in Fig. 2a, an asymmetric unit cell contains two 8–coordinated Sm^{3+} ions, one and a half of fully deprotonated $EBTC^{4-}$ ligands, four coordinated methanol molecules and six guest water molecules. Two crystallographically independent Sm^{3+} ions (labeled as Sm1 and Sm2, respectively) are coordinated with eight oxygen atoms, four from two bidentately coordinating carboxyl groups, two from two monodentately carboxyl groups, and the other two from two methanol molecules, however, show different coordination polyhedron. The coordination geometry around Sm1 ions can be described as dodecahedron while Sm2 ions show distorted trigonal dodecahedral geometries (Fig. 2b); the bond lengths and the angles in the coordinated polyhedra are

summarized in Table 3 and Table S2, from which it can be found that the Sm–O bond distances range from 2.266(5) to 2.493(5) Å, and the O–Sm–O bond angles span from 50.8(2) to 155.5(2)°. These bond parameters are similar to the values in Ln–carboxylate complexes in literature.[14] One of two different $EBTC^{4-}$ ligands (containing O10) possesses C_s point group symmetry, however, two phenyl rings in two different $EBTC^{4-}$ ligands are almost coplanar.

Table 3 Selected bond distances (Å) in **4, 5,** and **9**

			4		
Nd1–O1	2.387(4)	Nd1–O3	2.503(5)	Nd1–O4	2.452(4)
Nd1–O6	2.303(4)	Nd1–O9	2.509(4)	Nd1–O10	2.369(4)
Nd1–O13	2.372(4)	Nd1–O14	2.359(4)	Nd2–O2	2.297(4)
Nd2–O7	2.512(5)	Nd2–O15	2.361(4)	Nd2–O16	2.400(5)
Nd2–O5	2.372(5)	Nd2–O8	2.390(5)	Nd2–O11	2.410(5)
Nd2–O12	2.472(4)				
			5		
Sm1–O1	2.347(6)	Sm1–O3	2.459(6)	Sm1–O4	2.414(6)
Sm1–O6	2.266(5)	Sm1–O9	2.493(5)	Sm1–O10	2.325(6)
Sm1–O13	2.331(6)	Sm1–O14	2.330(6)	Sm2–O2	2.283(5)
Sm2–O5	2.365(7)	Sm2–O7	2.491(6)	Sm2–O8	2.348(6)
Sm2–O11	2.375(7)	Sm2–O12	2.441(6)	Sm2–O15	2.306(6)
Sm2–O16	2.383(6)				
			9		
Dy1–O6	2.281(3)	Dy1–O1	2.337(3)	Dy1–O13	2.339(3)
Dy1–O14	2.355(4)	Dy1–O10	2.356(4)	Dy1–O4	2.418(3)
Dy1–O3	2.462(4)	Dy1–O9	2.482(3)	Dy2–O2	2.278(3)
Dy2–O5	2.322(4)	Dy2–O8	2.348(4)	Dy2–O15	2.350(4)
Dy2–O16	2.382(4)	Dy2–O11	2.399(4)	Dy2–O12	2.449(4)
Dy2–O7	2.461(4)				

The adjacent two eight–coordinated Sm^{3+} centers (Sm1 and Sm2) in **5** are bridged together by two carboxylate groups (O1/C7/O2 and O5/C17/O6) from two different $EBTC^{4-}$ ligands, giving a dinuclear $[Sm_2(COO)_6]$ subunit (SBU), and the Sm1–Sm2 distance is 5.537Å within this SBU (Fig. 2a). The six $EBTC^{4-}$ ligands (represented as A, B, C, D, E and F, respectively) connected the neighboring SBUs exhibit three different orientations. As shown in Fig. 2c, the ligands A and B are parallel with each other; the ligand C is parallel to D, while the ligand E is approximately parallel to F, with a dihedral angle of 14.01°. The dihedral angles between the different orientated

ligands A and C, B and E, as well as C and F are 16.41°, 64.97° and 64.97°, respectively. Meanwhile, each $EBTC^{4-}$ ligand directly bridges six Sm^{3+} ions, or connects four dinuclear units, through its four carboxylate groups adopting bis–monodentate and chelated bidentate coordination modes, which can be clearly seen from Fig.2d. Namely, each $[Sm_2(COO)_6]$ SBU is surrounded by six $EBTC^{4-}$ bridged ligands and each $EBTC^{4-}$ ligand connects four $[Sm_2(COO)_6]$ SBUs, generating a three–dimensional (3–D) open framework (Fig.2e). The guest water molecules, being disordered, locate in the channels. All water and methanol molecules can be completely removed upon heating. The dimension of free channel along the *a*–axis is calculated as 8.7×12.2 Å when the van der Waals radii of the atoms at the wall of the channel were subtracted. The total potential void volume is 50.4% calculated from PLATON/SOLV[15] if the guest water and coordinated methanol molecules were removed. From the view point of topology, the 3–D structure of **5** can be described as a (4, 6)–connected network with Schläfli symbol of $\{3^{10}\}$ by reducing each SBU as a 6–connected node and the organic ligand serves as a 4–connected node (Fig. 2f).

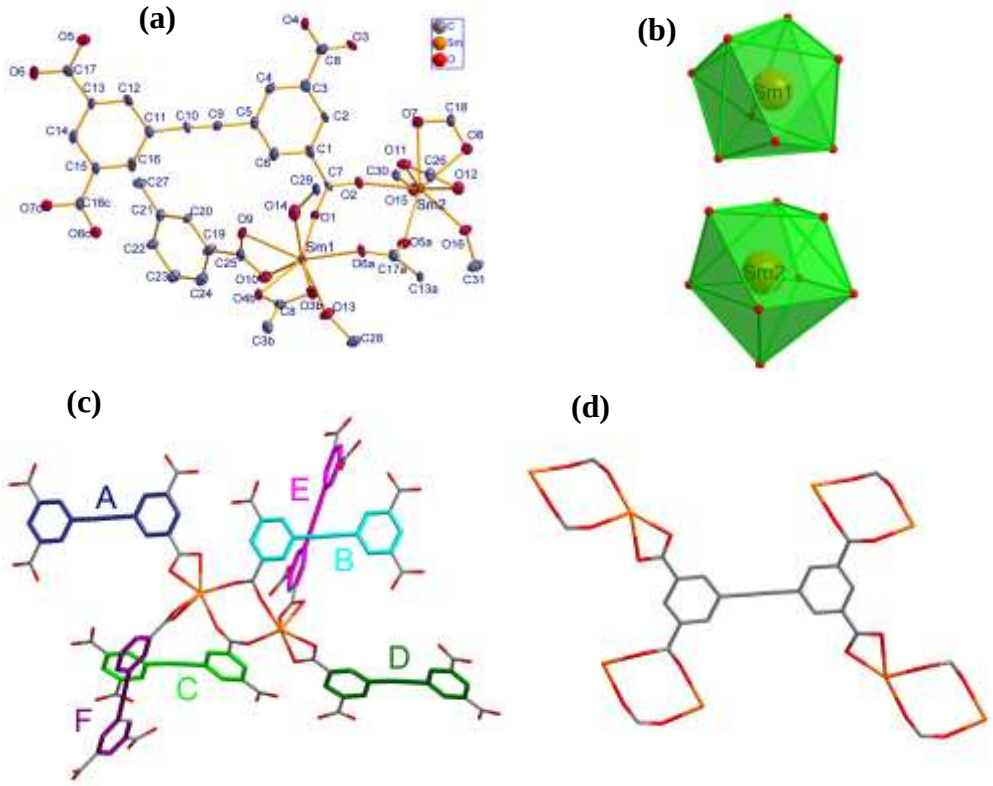

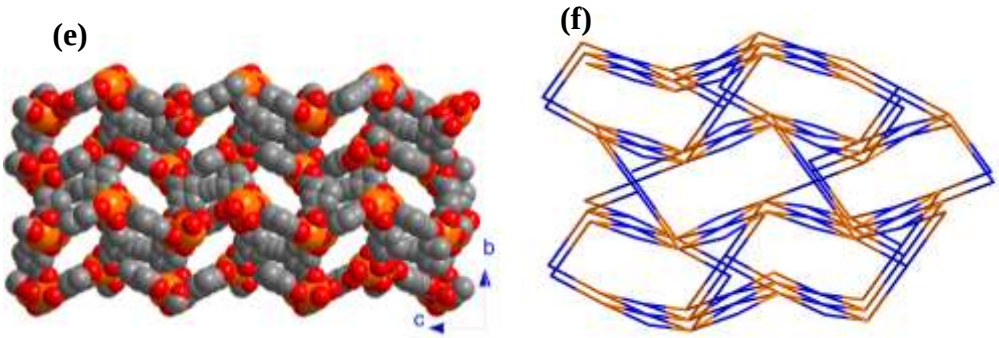

Fig. 2 (a) Coordination environments of Sm^{3+} ions with the H atoms omitted for clarity; Symmetry codes: a = 0.5+x, 0.5+y, -0.5+z; b = -0.5+x, 0.5+y, -0.5+z; c = -1+x, y, z; (b) coordination polyhedron of Sm^{3+} ions; (c) different orientations of $EBTC^{4-}$ ligands around dinuclear $[Sm_2(COO)_6]$ subunit (SBU); (d) connectivity of SBUs; (e) space filled representation of the 3–D framework viewed along the *a* axis; (f) (4,6) –connected network presented, orange represents the 6–connected node of SBU and blue represents the 4–connected node of organic ligand in **5**.

TG Analyses

The isomorphism **1–9** exhibit similar thermal behavior with several continuous weight loss processes below 400 °C, and these weight loss processes correspond to the guest water and coordinated methanol molecules releasing, which can be seen clearly from their TG curves in Fig. S4. As a representative example in Fig. 3, compound **5** shows a two–step sequential weight loss process with a percentage of 3.64 % before 73 °C, corresponding to the release of two guest water molecules within the framework (calcd 3.63 %), and 20.86 % in the temperature range of 73–387°C, attributing to the liberation of four residual guest water and four coordinated methanol molecules per formula unit (calcd 20.85 %). All lattice water and coordinated methanol molecules can be removed around 387 °C. Its framework will be gradually collapsed upon further heating. The decomposing temperature of most compounds is round 380 °C (ref. Fig.S4), such high thermal stability is related to the electronic structure of rare earth ion, where the open electronic shell (f–orbitals) are screened by higher closed–shells of s– and p–orbitals, leading to that the coordinating interactions are mainly contributed from the electrostatic interactions

between the positive charge rare earth ion and the negative charge carboxylates. Since the electrostatic interaction is without orientation, the binding strain arose from the coordination sphere change is easily released during the heating process, and this gives the highly thermal stability.

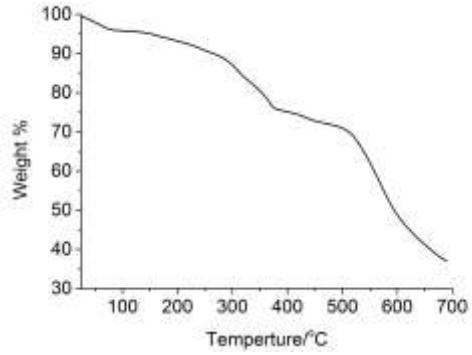

Fig. 3 The TG curve of **5**.

Photoluminescence Properties

Generally, the luminescence of a lanthanide coordination compound originates from the intraligand π←π* transition with broadband emission or the internal 4f–4f electronic transitions between the $^{2S+1}L_J$ energy levels with narrow, sharp and well−separated emission bands. For a Ce^{3+} coordination compound, an broadband emission band is often observed, and such an emission is due to the allowed f–d transitions. The emission arose from trivalent lanthanide (Ln^{3+} apart from Ce^{3+}) ions possesses high color purity, which is potential luminescent material.[16]

The photoluminesecence spectra of **1** and **7** in solid state at room temperature are given in Fig. 4, and their excitation spectra are given in Fig. S6(a) and (c). Both coordination polymers show a broadband emission centered at 556 nm under the excitation at 320 nm, such a broadband emission is assigned to the intraligand π←π* transition of $EBTC^{4-}$. While, as shown in Fig. S5, the emission band ascribed to the π←π* transition is centered at 436 nm (λ_{ex} = 320 nm) for **H_4EBTC** in solid state at room temperature. With respect to the emission of **H_4EBTC**, the π←π* transition band in **1** and **7** shifts towards the low energy side (red−shift), indicating that the ligand interactions upon coordination with the metal ion affect the HOMO and LUMO levels of ligand to change the transition energy.

The f–orbitals of the La^{3+} and Gd^{3+} ions are empty and half–filled, respectively; and the f–orbitals of the Sm^{3+}, Eu^{3+}, Tb^{3+} and Dy^{3+} ions are not completely filled, by comparison of the La^{3+} and Gd^{3+} ions, the Sm^{3+}, Eu^{3+}, Tb^{3+} and Dy^{3+} ions are prone to exhibit f–f transitions if the energy transfer is efficient between the π* orbital of ligand and f–orbital of lanthanide ion. As shown in Fig. 5a, coordination polymer **5** shows three characteristic emission bands of Sm^{3+} ion, centered at 562, 598, and 645 nm with orange luminescence excited at 265 nm. Three emission bands are corresponding to the $^4G_{5/2}\rightarrow{}^6H_{5/2}$, $^4G_{5/2}\rightarrow{}^6H_{7/2}$, and $^4G_{5/2}\rightarrow{}^6H_{9/2}$ characteristic transitions of the Sm^{3+} ion, respectively.[17]

The solid−state excitation spectrum of compound **6** is obtained by monitoring the emission of the $^5D_0\rightarrow{}^7F_2$ transition of the Eu^{3+} ions at 618 nm (Fig. S6(b)). It can be seen clearly that the excitation spectrum consists of two broad bands in 278 and 325 nm, ascribing to the $\pi\rightarrow\pi^*$ transition of the ligand and the energy transfer from the ligand to the metal, respectively. The other weak sharp excitation peaks at 361, 375, 382 and 395 nm can be attributed to $^5H_4\leftarrow{}^7F_{0,1}$, $^5D_4\leftarrow{}^7F_{0,1}$, $^5G_{2-6}\leftarrow{}^7F_{0,1}$, $^5L_6\leftarrow{}^7F_{0,1}$, $^5D_2\leftarrow{}^7F_{0,1}$ and $^5D_1\leftarrow{}^7F_{0,1}$ transitions. When excited at 278 nm, it displays characteristic red luminescence of Eu^{3+} ion in the visible region (ref. the CIE chromaticity diagram Fig. 6), and five emission bands are centered at 581, 595, 618, 654 and 701 nm (Fig. 5b), which are assigned to the transitions of Eu^{3+} ion: $^5D_0\rightarrow{}^7F_0$ (581 nm), $^5D_0\rightarrow{}^7F_1$ (595 nm), $^5D_0\rightarrow{}^7F_2$ (618 nm), $^5D_0\rightarrow{}^7F_3$ (654 nm), $^5D_1\rightarrow{}^7F_5$ (691 nm), and $^5D_0\rightarrow{}^7F_4$ (701 nm) transitions.[18] Among them, the symmetric forbidden emission $^5D_0\rightarrow{}^7F_0$ around 581 nm is almost invisible, the magnetic–dipolar $^5D_0\rightarrow{}^7F_1$ transition around 595 nm exhibits medium–strong emission, while the electric–dipolar $^5D_0\rightarrow{}^7F_2$ transition at 618 nm displays the most intense emission. Moreover, the magnetic dipole transition around 654 nm ($^5D_0\rightarrow{}^7F_3$) and electric dipole transition around 701 nm ($^5D_0\rightarrow{}^7F_4$) are also very weak and could hardly be observed. Usually, the intensity ratio $I(^5D_0\rightarrow{}^7F_2):I(^5D_0\rightarrow{}^7F_1)$ is indicative of the local symmetry of the coordination sphere around the Eu^{3+} ions. For high symmetry, the emission spectrum is dominated by the $^5D_0\rightarrow{}^7F_1$ transition, while for low symmetry the $^5D_0\rightarrow{}^7F_2$ transition is much more intense since the electric-dipolar $^5D_0\rightarrow{}^7F_2$

transition is hypersensitive to the coordination environment of the Eu^{3+} ions. [19] As for **6,** the intensity ratio of $^5D_0 \rightarrow {}^7F_2/{}^5D_0 \rightarrow {}^7F_1$ is ca. 6, indicating that the Eu^{3+} ions are not located at the inversion center with low site symmetry,[20] and in agreement with the crystal structure analysis.

In the emitting spectrum of **8**, four characteristic bands arising from f–f transitions of Tb^{3+} ion are observed at 492, 546, 587, and 622 nm when excited at 320 nm (Fig. 5c, its excitation spectrum is given in Fig. S6(d)), and these emissions are attributed to $^5D_4 \rightarrow {}^7F_J$ (J = 6, 5, 4 and 3) transitions respectively. The green color luminescence (ref. the CIE chromaticity diagram Fig. 6) is due to the dominating Tb^{3+} emission at 546 nm. Compound **9** also displays the typical emission of Dy^{3+} ions when excited at 320 nm (Fig. 5d, its excitation spectrum is given in Fig. S6(e)). The emission bands at 483 and 576 nm can be attributed to the $^4F_{9/2} \rightarrow {}^6H_J$ (J = 15/2 and 13/2) transitions of Dy^{3+} ions respectively, while the $^4F_{9/2} \rightarrow {}^6H_{11/2}$ band was not observed.

Upon excitation at 350 nm, compound **4** gives rise to three typical emission bands in the NIR region within the 880−1368 nm range (Fig. 5e). The main emission bands occur between 1028 and 1096 nm, with a maximum at 1058 nm (corresponding to the transition $^4F_{3/2} \rightarrow {}^4I_{11/2}$). The other two bands appear within 880−1012 nm ($^4F_{3/2} \rightarrow {}^4I_{9/2}$) and 1176−1366 nm ($^4F_{3/2} \rightarrow {}^4I_{13/2}$), respectively. The emission bands around 1058 and 1336 nm have an important application in NIR laser system and telecommunication, reepectively.[21] As a result, this coordination polymer is expected to have potential application in the above–mentioned technique fields. The $^4F_{3/2} \rightarrow {}^4I_{9/2}$ emission in **4** presents splitting, which is mainly attributed to "crystal-field effects" of Nd^{3+} ion in a C1 symmetry.[22]

Compound **2** presents a light blue emission (ref. the CIE chromaticity diagram Fig. 6), and two broad emission bands are centered at 468 and 491 nm (Fig. 5f), respectively. The Ce^{3+} ion is the only trivalent lanthanide ion, which exhibits reduction of the energy of 5d states by splitting of the crystal and ligand fields that enables 4f→5d excitation within the UV region close to the visible and 5d→4f emission in the visible region of the spectrum.[23]

It is worth noting that usually the characteristic emission bands are located in the

NIR region for Pr^{3+} ion, while no NIR emission band was found for **3**. In addition, no remnant H_4EBTC–based emission is observed in the emission spectra of **2, 4–6, 8** and **9.** The disappearance of the organic ligand emission band in these coordination polymers established that there exists an effective energy transfer between the π* level of ligand and the f–level of lanthanide ion, and the $EBTC^{4-}$ ligand is an effective antenna ligand for constructing highly efficient luminescence lanthanide complexes.

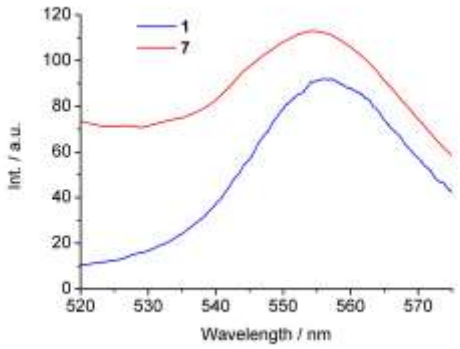

Fig. 4 Emission spectra of **1** and **7** under excitation λ_{ex} = 320 nm at room temperature

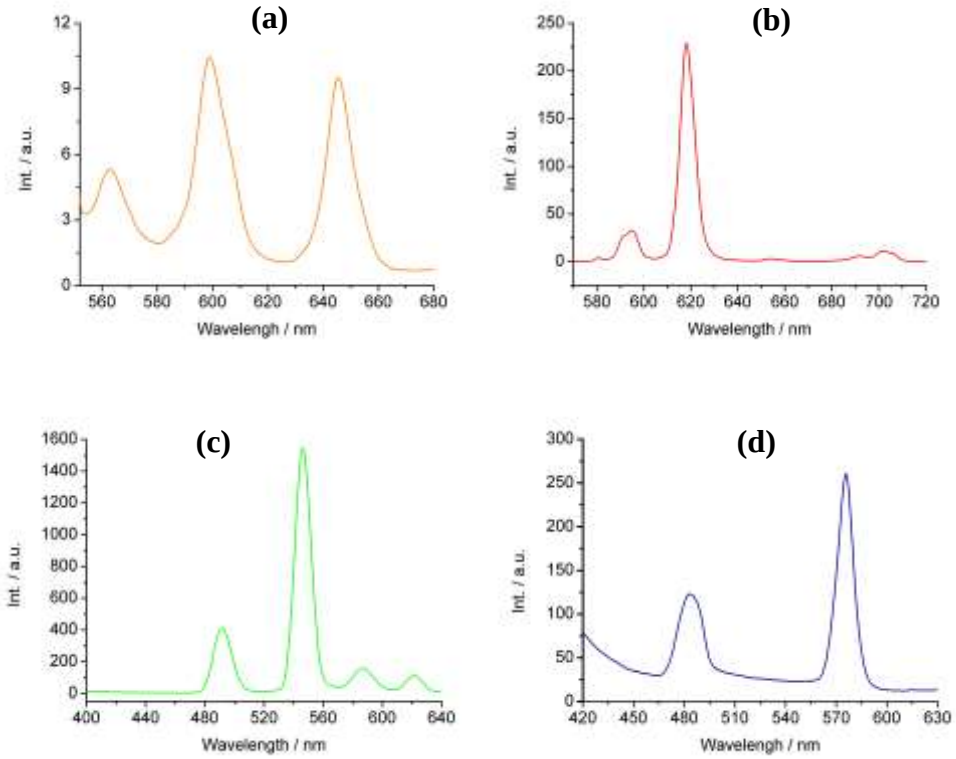

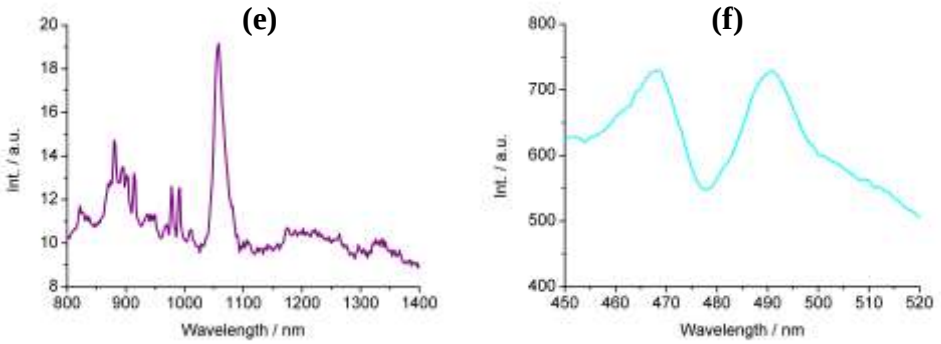

Fig. 5 Emission spectra of **5** (a), **6** (b), **8** (c) and **9** (d), NIR emission spectra of **4** (e) and **2** (f).

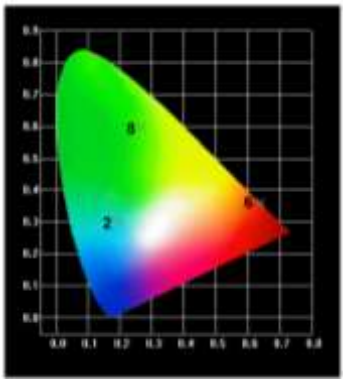

Fig. 6 CIE chromaticity diagram for **2**, **6** and **8**

The photoluminescence lifetime, τ, of **1**, **4**, **5**, **6, 8** and **9** were further investigated in the solid state at room temperature. Fig. 7 shows the luminescence decay profiles of them. The process of photoluminescence decay follows a single exponential decay law, as a result, the Eq. (1) was utilized for fitting the curves of photoluminescence decay:

$$y = y_0 + A_1 \times \exp(-t/\tau) \qquad (1)$$

In Eq. (1), y_0 and A_1 are two constants, and τ is the decay constant, representing photoluminescence lifetime. The best fits were performed to give τ = 2.43 μs for **1**, 1.85 μs for **4**, 1.69 μs for **5**, 0.84 ms for **6**, 0.39 ms for **8** and 1.85 μs for **9**, respectively. Usually, the f–f electronic transitions of lanthanide ion are forbidden, leading to long excited state decay time. In this study, it was found that the photoluminescence lifetimes of **6** and **8** are at millisecond magnitude order, falling in the range of lanthanide ion photoluminescence decay time 10–2000 μs. It should be

noted that only a few coordination polymers have been reported to exhibit a millisecond time scale.[24]

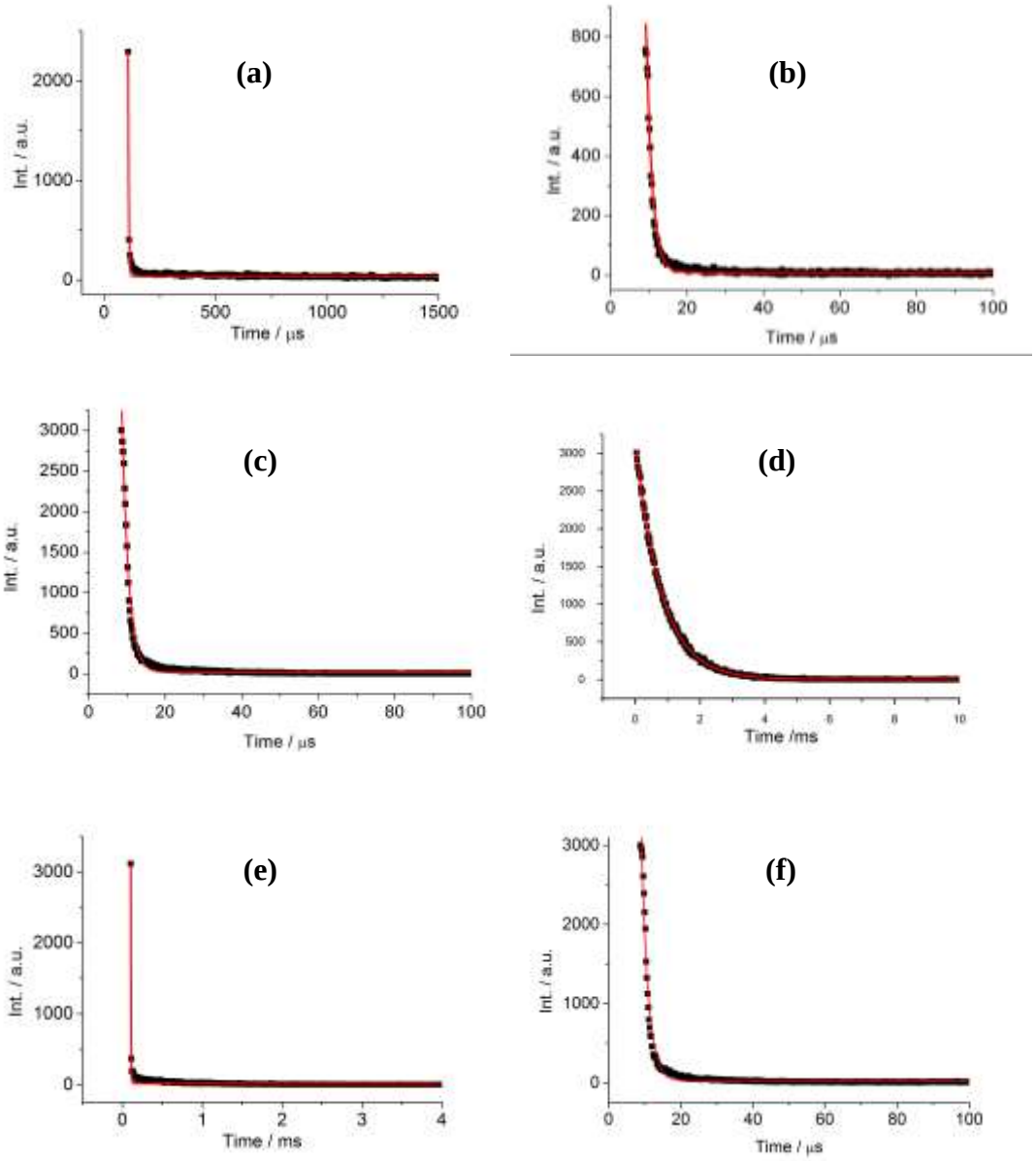

Fig.7 Luminescence decay profiles obtained at room temperature upon pulsed excitation at 320 nm for (a) **1**, (b) **4**, (c) **5**, (d) **6**, (e) **8**, and (f) **9**. The main emission peaks at 556 nm, 1058 nm, 598 nm, 618 nm, 546 nm and 576 nm were monitored, respectively. The red lines represent the fitting curves and the black lines are the raw experimental data.

Conclusion

In summary, nine isostructural lanthanide–MOFs were successfully prepared

using the conjugated $EBTC^{4-}$ ligand with lanthanide nitrate via solvothermal reaction. In each lanthanide–MOF, two lanthanide ions (Ln = La, Ce, Pr, Nd, Sm, Eu, Gd, Tb and Dy) are bridged by two carboxylates to form $[Ln_2(COO)_6]$ dinuclear subunit (SUB); each SUB is surrounded by six $EBTC^{4-}$ bridged ligands and each $EBTC^{4-}$ ligand connects four SUBs, generating a 3–D (4, 6)–connected network with Schläfli symbol of $\{3^{10}\}$.

The lanthanide–MOFs (Ln = Nd, Sm, Eu, Tb and Dy**)** displayed luminescence in solid state at room temperature and the emissions exhibit the typical f–f transitions of Nd^{3+}, Sm^{3+}, Eu^{3+}, Tb^{3+} and Dy^{3+} ions, respectively. Compound **2** (Ln = Ce) shows a light blue emission due to the $5d \rightarrow 4f$ transition. These results indicated the conjugated $\mathbf{EBTC}^{4-}$ anion is a good 'antenna effect' ligand for constructing luminescent lanthanide–MOFs. Compounds **1** (Ln = La) and **7** (Ln = Gd) show a green emission due to the intraligand $\pi \leftarrow \pi^*$ transition. It is worth mentioning that **6** (Ln = Eu) and **8** (Ln = Tb) show lifetimes at millisecond levels, and such lanthanide–MOFs may become promising candidates for time–resolved photoluminescence anisotropy measurement and application in the research of biomacromolecule.

Acknowledgments

Authors thank National Nature Science Foundation of China for financial support (grant no. 91122011, 51173075 and 21271103).

Electronic Supplementary Information (ESI)

CCDC 1037093, 1037094 and 1037095 contain the supplementary crystallographic data for **4**, **5** and **9**, respectively. These data can be obtained free of charge from The Cambridge Crystallographic Data Centre via www.ccdc.cam.ac.uk/data_request/cif. The preparation of **2–9** is detailed in the supporting material. Cell Parameters of Compounds $C_{31}H_{29}Ln_2O_{18}$ (Ln = La (**1**), Ce (**2**), Pr (**3**), Nd (**4**), Sm (**5**), Gd (**7**), Dy (**9**) are given in Table S1. Selected bond angles of **4, 5** and **9** are listed in Table S2.

Crystallographic data, structural refinements and selected bond lengths and angles for **1** and **3** are given in Table S3 and Table S4, respectively. PXRD patterns of **3**, **4**, **5** and **9** are plotted in Fig. S1. The IR spectra of **1–9** are presented in Fig. S2. The crystal structure of **4** and **9** is shown in Fig. S3. The TG curves of **1–9** are presented in Fig. S4. The UV−vis absorption and emission spectra of ligand H_4EBTC are shown in Fig. S5. The excitation spectra of **1**, **6**, **7**, **8** and **9** are shown in Fig. S6. For ESI and crystallographic data or other electronic format see DOI: ??????????????

References

1. M. Eddaoudi, J. Kim, N. Rosi, D. Vodak, J. Wachter, M. O'Keeffe and O. M. Yaghi, *Science*, 2002, **295**, 469.
2. (a) B. L. Chen, S. Q. Ma, E. J. Hurtado, E. B. Lobkovsky and H. C. Zhou, *Inorg. Chem.*, 2007, **46**, 8490; (b) J.–R. Li, R. J. Kuppler and H.–C. Zhou, *Chem. Soc. Rev.*, 2009, **38**, 1477; (c) S.–i. Noro, T. Akutagawa and T. Nakamura, *Chem. Commun.*, 2010, **46**, 3134; (d) M. C. Das, Q. S. Guo, Y. B. He, J. Kim, C.–G. Zhao, K. L. Hong, S. C. Xiang, Z. J. Zhang, K. M. Thomas, R. Krishna and B. L. Chen, *J. Am. Chem. Soc.*, 2012, **134**, 8703.
3. (a) N. L. Rosi, J. Eckert, M. Eddaoudi, D. T. Vodak, J. Kim, M. O'Keeffe and O. M. Yaghi, *Science*, 2003, **16**, 1127; (b) C. Wang, D. M. Liu and W. B. Lin, *J. Am. Chem. Soc.*, 2013, **135**, 13222; (c) P. Zhang, B. Li, Y. Zhao, X. G. Meng and T. L. Zhang, *Chem. Commun.*, 2011, **47**, 7722; (d) S.–i. Noro, T. Ohba, K. Fukuhara, Y. Takahashi, T. Akutagawa and T. Nakamura, *Dalton Trans.*, 2011, **40**, 2268; (e) K. Takahashi, N. Hoshino, T. Takeda, S.–i. Noro, T. Nakamura, S. Takeda and T. Akutagawa, *Dalton Trans.*, 2014, **43**, 9081.
4. (a) B. L. Chen, Y. Yang, F. Zapata, G. D. Qian, Y. S. Luo, J. H. Zhang and E. B. Lobkovsky, *Inorg. Chem.*, 2006, **45**, 8882; (b) Y. J. Cui, Y. F. Yue, G. D. Qian and B. L. *Chen, Chem. Rev.*, 2012, **112**, 1126; (c) L. V. Meyer, F. Schönfeld and K. Müller-Buschbaum, *Chem. Commun.*, 2014, **50**, 8093; (d) J. M. Zhou, W. Shi, N. Xu and P. Cheng, *Inorg. Chem.*, 2013, **52,** 8082; (e) M. D. Allendorf, C. A. Bauer, R. K. Bhakta and R. J. T. Houk, *Chem. Soc. Rev.*, 2009, **38**, 1330.

5. (a) C. Dey, R. Das, B. K. Saha, P. Podda and R. Banerjee, *Chem. Commun.*, 2011, **47**, 11008; (b) M.-X.Hu, Y.–G. Chen, C.–J. Zhang and Q.–J. Kong, *CrystEngcomm*, 2010, **12**, 1454; (c) S. K. Langley, N. F. Chilton, B. Moubaraki and K. S. Murray, *Chem. Commun.*, 2013, **49**, 6965; (d) M. Kurmoo, *Chem. Soc. Rev.*, 2009, **38**, 1353.
6. (a) X.–Y. Dong, R. Wang, J.–B. Li, S.–Q. Zang, H.–W. Hou and T. C. W. Mak, *Chem. Commun.*, 2013, **49**, 10590; (b) R. Wang, X. –Y. Dong, H. Xu, R. –B. Pei, M.–L. Ma, S.–Q. Zang, H.–W. Hou and T. C. W. Mak, *Chem. Commun.*, 2014, **50**, 9153.
7. (a) X.–Y. Dong, B. Li, B.–B. Ma, S.–J. Li, M.–M. Dong, Y.–Y. Zhu, S.–Q. Zang, Y. Song, H.–W. Hou and T. C. W. Mak, *J. Am. Chem. Soc.*, 2013, **135**, 10214; (b) C. Pan, J. Nan, X. Dong, X. M. Ren and W. Jin, *J. Am. Chem. Soc.*, 2011, **133**, 12330.
8. (a) K. Binnemans, *Chem. Rev.*, 2009, **109**, 4283; (b) F. J. Steemers, W. Verboom, D. N. Reinhoudt, E. B. vander Tol and J. W. Verhoeven, *J. Am. Chem. Soc.*, 1995, **117**, 9408.
9. (a) M.–Li. Ma, C. Ji and S.–Q. Zang, *Dalton Trans.*, 2013, **42**, 10579; (b) M. S. Liu, Q. Y. Yu, Y.P. Cai, C. Y. Su, X. M. Lin, X. X. Zhou and J. W. Cai, *Cryst. Growth Des.*, 2008, **8**, 4083; (c) T. F. Liu, W. Zhang, W. H. Sun and R. Cao, *Inorg. Chem.*, 2011, **50**, 5242; (d) J. Yang, Q. Yue, G. D. Li, J. J. Cao, G. H. Li and J. S. Chen, *Inorg. Chem.*, 2006, **45**, 2857; (e) X. D. Guo, G. S. Zhu, Z. Y. Li, Y. Chen, X. T. Li and S. L. Qiu, *Inorg. Chem.*, 2006, **45**, 4065.
10. L. F. Wang, L. C. Kang, W. W. Zhang, F. M. Wang, X. M. Ren and Q. J. Meng, *Dalton Trans.*, 2011, **40**, 9490.
11. Y. X. Hu, S. C. Xiang, W. W. Zhang, Z. X. Zhang, L. Wang, J. F. Bai and B. L. Chen, *Chem. Commun.*, 2009, **48**, 7551.
12. *Software packages SMART and SAINT*, Siemens Analytical X-ray Instrument Inc., Madison, WI, 1996.
13. G. M. Sheldrick, *SHELX–97, Program for the refinement of crystal structure*, University of Göttingen, Germany, 1997.
14. (a) H. S. Wang, B. Zhao, B. Zhai, W. Shi, P. Cheng, D. Z. Liao and S. P. Yan, *Cryst. Growth Des.*, 2007, **7**, 1851; (b) J. Xu, J. Cheng, W. Su and M. Hong,

Cryst. *Growth Des.*, 2011, **11**, 2294.

15. A. L. Spek, *J. Appl. Crystallogr.* 2003, ***36***, 7.
16. (a) B. L. Chen, L.–B. Wang, F. Zapata, G.–D. Qian and E. M. Lobkovsky, *J. Am. Chem. Soc.* 2008, **130**, 6718; (b) W. S. Liu, T. Q. Jiao, Y. Z. Li, Q. Z. Liu, M. Y. Tan, H. Wang and L. F. Wang, *J. Am. Chem. Soc.* 2004, **126**, 2280.
17. P. Wang, R.–Q. Fan, X.–R. Liu, L.–Y. Wang, Y.–L. Yang, W.–W. Cao, B. Yang, W. Hasi, Q. Su and Y. Mu, *CrystEngcomm.*, 2013, **15**, 1931.
18. (a) D. P. Dong, L. Liu, Z. G. Sun, C. Q. Jiao, Z. M. Liu, C. Li, Zhu, Y. Y. K. Chen and C. L. Wang, *Cryst. Growth Des.*, 2011, **11**, 5346; (b) R. Feng, L. Chen, Q. H. Chen, X. C. Shan, Y. L. Gai, F. L. Jiang and M. C. Hong, *Cryst. Growth Des.*, 2011, **11**, 1705; (c) S. Dang, E. Ma, Z. Sun and H. Zhang, *J. Mater. Chem.*, 2012, **22,** 16920; (d) J. Xia, B. Zhao, H. S. Wang, W. Shi, Y. Ma, H. B. Song, P. Cheng, D. Z. Liao and S. P. Yan, *Inorg. Chem.*, 2007, **46**, 3450; (e) A. K. Singh, S. K. Singh, H. Mishra, R. Prakash and S. B. Rai, *J. Phys. Chem. B* 2004, **114**, 13042.
19. H. J. Zhang, X. Z. Wang, D. R. Zhu, Y. Song, Y. Xu, H. Xu, X. Shen, T. Gao and M. X. Huang, *CrystEngComm.*, 2011, **13**, 2586.
20. (a) J. W. Cheng, S. T. Zheng and G. Y. Yang, *Dalton Trans*., 2007, 4059; (b) Y. Q. Sun, J. Zhang and G. Y. Yang, *Chem. Commun.*, 2006, 4700.
21. (a) J. C. G. Bunzli and C. Pigue, *Chem. Soc. Rev.*, 2005, **34**, 1048; (b) D. Jaque, O. Enguita, J. García Solé, A. D. Jiang and Z. D. Luo, *Appl. Phys. Lett.*, 2000, **76**, 2176.
22. S. Chen, R. Q. Fan, C. F. Sun, P. Wang, Y. L. Yang, Q. Su and Y. Mu, *Cryst. Growth Des.* 2012, **12**, 1337.
23. G. Blasse and B. C. Grabmaier, *Luminescent Materials;* Springer Verlag: Berlin, Germany, 1994.
24. A. Rodríguez–Dié guez, A. Salinas–Castillo, A. Sironi, J. M. Seco and E. Colacio, *CrystEngComm*, 2010, **12**, 1876.